Absence of Lateral Phase Segregation in Fatty Acid-Based Catanionic Mixtures

Youlia Michina,[†] David Carrière,*[,†] Thibault Charpentier,[‡] Rodrigo Brito,[§] Eduardo F. Marques,[§] Jean-Paul Douliez,[||] and Thomas Zemb[⊥]

CEA, IRAMIS, SIS2M, LIONS (Laboratoire Interdisciplinaire sur l'Organisation Nanométrique et Supramoléculaire), F-91191 Gif-sur-Yvette cedex, France, CEA, IRAMIS, SIS2M, LSDRM (Laboratoire Structure et Dynamique par Résonance Magnétique), F-91191 Gif-sur-Yvette cedex, France, Centro de Investigação em Qumica, Department of Chemistry, Faculty of Sciences, University of Porto, Rua do Campo Alegre, no. 687, 4169-007 Porto, Portugal, UR1268 Biopolymères Interactions Assemblages, INRA équipe ISD, Rue de la Géraudière, 44316 Nantes, France, and CEA, CNRS, ICSM, Univ UMR 5257, F-30207 Bagnols Sur Ceze, France

Received: October 27, 2009; Revised Manuscript Received: December 9, 2009

Mixtures of ionic surfactants of opposite charge ("catanionic" mixtures) show strongly nonideal behaviors, for example, in terms of evolution of surface tension, critical micelle concentration, or morphology with respect to composition in each surfactant. In several catanionic systems, it has been proposed that the interaction between both surfactants is so strong that lateral phase segregation occurs within bilayers, with crystallites of preferential composition demixing from the excess of the other surfactant. Here, we investigate the temperature−composition phase diagram of the myristic acid/cetyltrimethylammonium mixtures. Combining microcalorimetry, X-ray diffusion, and solid-state deuterium NMR, we demonstrate that no separation is observed in the gel (L_β) state. The catanionic mixtures therefore behave like two-dimensional solid solutions with a negative azeotrope: the existence of a composition at which a maximum in melting temperature is observed does not imply the existence of a preferential crystal of this composition, but results from the preferential attraction between unlike amphiphilic molecules. Additionally, this study reveals the presence of a so-called intermediate phase, that is, a phase that shows dynamic properties intermediate between that of the L_β and the L_α phases.

Introduction

Mixtures of surfactants of opposite charge, also called "catanionic" mixtures, self-assemble into a large variety of structures, for example, mixed micelles, lamellar phases, nano- and microdiscs, vesicles, and bicontinuous structures.[1−8] The strong interactions between surfactant molecules lead to highly nonideal, synergetic behaviors regarding the critical micelle concentration, surface tension, molar volume, solubilization, viscosity, and so on.[9−15] The regular solution theory qualitatively describes some of these results,[16] but more advanced models are often required.[17−20] Of particular interest is the variation of the aggregate composition against the bulk composition of the mixture, as it determines the charge, size, curvature, and so on of the surfactant assembly. Usually, the aggregate composition is getting closer to equimolarity as the total surfactant concentration[21−24] or the added salt concentration[25] decreases. This effect is well described by the different proposed theoretical treatments,[26,27] and it results from the competition between electrostatic forces, that favor equimolarity, and entropy of mixing, that tend to reduce the difference between bulk and aggregate composition.

However, a very strong deviation from this general behavior has been reported recently. Mixtures of linear fatty acids ($C_{n-1}COOH$) and linear alkyl trimethylammonium bromide or chloride ($C_mTA^+X^-$, $X^- = Br^-, Cl^-$) show a critical ratio $f_{crit} = C_{n-1}COOH/(C_mTAX + C_{n-1}COOH) \sim 2/3$ (i.e., 2 fatty acids per cationic surfactant) that determines several intriguing properties. In particular, upon dialysis, mixtures initially richer in cationic surfactant ($f_0 < f_{crit}$) will lose cationic surfactant until f_{crit} is reached and assemble into bilayers that form aggregates with no specific morphology at the micrometer scale.[28] In mixtures initially richer in fatty acid ($f_0 > f_{crit}$), f remains constant during the dialysis; that is, no cationic surfactant is extracted despite a solubility several orders of magnitudes higher than that of the linear fatty acid. Additionally, only such mixtures prepared at $f_0 > f_{crit}$ form micrometer-size vesicles highly resistant to dialysis which spontaneously "self-encapsulate" the H^+X^- ions released upon surfactant association.[28,29] The origin of this critical ratio is still unclear and has to be decided between several possible explanations.

Here, we examine if the observation of f_{crit} in the myristic acid/cetyl trimethylammonium bromide mixtures ($n = 14$, $m = 16$) results from the formation of a preferential compound of composition $f = f_{crit}$ that spontaneously segregates from the excess surfactant in the bilayer, with the latter having the possibility to be extracted by dialysis. Such a lateral segregation at the micrometer scale between a preferential compound and the rest of the surfactant has already been invoked to explain the faceting of vesicles in mixtures of cetyltrimethyl ammonium hydroxide with a slight excess of myristic acid ($C_{16}TAOH/C_{13}COOH$)[30] and in mixtures of sodium dodecyl sulfate and didodecyldimethylammonium bromide (SDS/DDAB) upon addition of hydrophobically modified polymer.[31−33] Alternatively, both surfactants may be fully miscible in the bilayer at all compositions, but the cohesive energy of the bilayer might

* To whom correspondence should be addressed. E-mail: david.carriere@cea.fr. Telephone: +33 (0)1 69 08 54 89. Fax: +33 (0)1 69 08 66 40.
[†] CEA, IRAMIS, SIS2M, LIONS.
[‡] CEA, IRAMIS, SIS2M, LSDRM.
[§] University of Porto.
[||] UR1268 Biopolymères Interactions Assemblages.
[⊥] CEA, CNRS, ICSM.

10.1021/jp910267v
Published on Web 01/14/2010

continuously increase until the value becomes too high to allow any surfactant extraction. In this case, the critical ratio would not coincide with the segregation of bilayer patches with a preferential composition. To distinguish between both cases, we determine the composition−temperature phase diagram using microcalorimetry and assign the different phases with deuterium NMR performed on the perdeuterated system. Microcalorimetry has already been performed on a very similar system ($C_{13}COOH$/$C_{16}TAOH$[34]), but no conclusion could be drawn about possible lateral segregation. In the present study, a careful analysis of the thermograms and NMR spectra provides valuable information about the different phase separation processes within the bilayer upon temperature changes, the tie lines, and the structure and dynamics of the various phases.

Methods

Sample Preparation. The samples were prepared as described previously.[28] Known amounts of myristic acid ($C_{13}COOH$, Fluka, recrystallized in hot acetonitrile) and cetyltrimethylammonium bromide ($C_{16}TA^+Br^-$, Sigma, as such) are cosolubilized by stirring in Milli-Q water at 50 °C for 3 days. The solutions are prepared at variable surfactant ratios, with a total composition of 1% weight in water. The milky, birefringent solution is then transferred to a dialysis cassette (Pierce regenerated cellulose membranes, 3500 Da cutoff) and dialyzed at room temperature against a 100-fold volume of Milli-Q water which is changed typically after 1, 4, 24, and 48 h and 5 days of dialysis. Samples richer in $C_{16}TA^+$ have been prepared from higher contents in $C_{16}TAB$ and by stopping the dialysis at shorter times (Supporting Information). For ^2H NMR spectrometry, the samples are prepared with perdeuterated myristic acid (*d*-27 $C_{13}COOH$, Sigma) instead of hydrogenated myristic acid.

Differential Scanning Calorimetry (DSC). DSC scans were performed with a Setaram microDSCIII high-sensitivity calorimeter. Two steel batch cells were used, one containing ca. 0.8 mL of sample and the other, filled with the same amount of water, used as reference. The samples were scanned at 0.5 ° C min^{-1} in the 25−70 °C range. Origin 7.5 software was used to deconvolute the DSC curves by two Gaussians as discussed below.

The effective cooperative unit size n of transition from a compound A to a compound B gives a qualitative estimate for the crystallite size involved in the $A \rightarrow B$ transition. It was determined from

$$n = \frac{\Delta H_{vH}}{\Delta H_{cal}}$$

where ΔH_{cal} is the calorimetric enthalpy determined by integration of the deconvoluted endothermic peak and ΔH_{vH} is the Van't Hoff enthalpy.[35]

ΔH_{vH} is calculated from

$$\frac{\Delta H_{vH}}{RT^2} = \left(\frac{\partial \ln K}{\partial T}\right)_p$$

where K is the equilibrium constant of the $A \rightarrow B$ transition, as defined by

$$K(T) = \frac{A}{B}$$

with the relative amounts of A and B being determined by integration of the endothermic peak.

If the endothermic peak has a Gaussian shape centered on T_m and of standard deviation σ, then $(\partial \ln K/\partial T)|_p$ takes the following analytical form:

$$\left(\frac{\partial \ln K}{\partial T}\right)_p = \sqrt{\frac{8}{\pi}} \frac{\exp\left(-\frac{(T - T_m)^2}{2\sigma^2}\right)}{\sigma\left(1 - \left(\mathrm{erf}\left(\frac{T - T_m}{\sqrt{2\sigma}}\right)\right)^2\right)}$$

yielding

$$n = \sqrt{\frac{8}{\pi}} \frac{RT^2}{\sigma \Delta H_{cal}}$$

Evaluation of n by using this formula or by determining ΔH_{vH} from the experimental data did not qualitatively change the results.

^2H Solid State NMR Spectroscopy. Deuterium solid state NMR spectra were collected at variable temperature from 300 to 340 K on a 300 MHz Avance II Bruker spectrometer (magnetic field 7.04 T) operating at a frequency of 45.97 MHz. A broadband double channel HX probe was used with an adapted coil for loading a ZrO_2 7 mm rotor (used in magic-angle spinning experiments). The typical amount of sample was 500 μL. A solid echo sequence ($90-\tau-90-\tau$ acquisition) was used in order to collect spectra without baseline distortion, with 90° pulse length of 10 μs, interpulse delay of 20 μs, and recycle delays of 1s. Typically 2048−8192 scans were accumulated.

Data were processed using home built software (Gaussian apodization, Fourier transform, phase correction). For deuterium spectroscopy, the general theory for lipid systems can be found in the literature.[36] Briefly, the deuterium NMR spectrum is composed of doublets with a splitting, $\Delta\nu$, which depends on the orientation of the C−D bond with respect to the magnetic field. In an anisotropic but *disoriented* medium, all the orientations are allowed and these doublets are superimposed to form a powder spectrum having two main peaks with an increased intensity corresponding to the 90 orientation, separated by $\Delta\nu_{90}$. The edge of the spectrum corresponds to the 0 orientation, with a splitting $\Delta\nu_0$ equal to twice $\Delta\nu_{90}$. In the case of perdeuterated systems, the spectrum is composed by the superimposition of signals from each labeled position.

In the case of a partially oriented anisotropic medium, a numerical procedure, generally called *de-Pakeing* or *inversion* was used to extract from the experimental spectra the underlying distribution of quadrupolar couplings.[37] Numerically, a Tikhonov regularization algorithm[38] with positiveness and smoothness constraints was employed as implemented in a homemade program.[39]

Briefly, in order to extract from the deuterium experimental spectrum $I(\upsilon)$ the distribution of quadrupolar couplings, say $\pi(C_Q)$, one has to solve the ill-posed problem (Fredholm integral of the first kind)

$$I_{exp}(\upsilon) = \int \mathrm{d}C_Q\, \pi(C_Q)\, I_{SIM}(\upsilon; C_Q, p(\theta)) \qquad (1)$$

where $I_{SIM}(\upsilon; C_Q, p(\theta))$ is the theoretical spectrum simulated with the quadrupolar coupling constant C_Q. The quadrupolar

asymmetry parameter is set to zero because of the axial symmetry of the motion, and $p(\theta)$ is the distribution function of θ, the angle between the axis of symmetry of motion and the external magnetic field. Equation 1 is solved by minimizing the functional $L(\pi)$:

$$L(\pi) = \frac{\chi^2}{2} + \lambda||\pi^{(2)}||^2, \quad \pi \geq 0 \qquad (2)$$

The first term is the usual least-squares term (ensuring compatibility of the fit with the experimental data), and the second term controls the smoothness (minimization of the second-order derivative of π). The minimization is restricted to positive π. Here, the *small* control parameter λ was adjusted manually (visual inspection of π) to a single value for all spectra from the same sample. A Boltzmann distribution was chosen for $p(\theta)$:

$$p(\theta)\alpha \sin\theta \exp\{k_B \cos^2\theta\}$$

with $k_B = 1$ determined so as to provide the best fit (minimum of χ^2). The obtained distribution π was found to be not very sensitive to small variations of k_B.

Before the de-Pakeing procedure, in order to minimize experimental imperfection, each spectrum is symmetrized around its center of gravity (all CD_x units are found to have the same isotropic chemical shift), which is determined without taking into account the narrow D_2O peak. The latter is also removed from the inversion analysis by choosing a small (but nonzero) lower bound for the C_Q values. In the coexistence regions, the relative amount of each phase was determined by integration of the peaks assigned to each respective CD_3 group.

Results

The $C_{13}COOH/C_{16}TA^+Br^-$ mixtures are prepared at variable initial myristic acid fractions f, as defined by

$$f = \frac{[C_{13}COOH]}{[C_{13}COOH] + [C_{16}TABr]}$$

As shown before,[28] the composition of the mixture (e.g., f and total surfactant concentration) as determined by HPLC depends on the initial molar fraction and on the duration of dialysis. Combining both parameters, samples with f in the 0.48−0.67 range have been prepared (Supporting Information). The corresponding micro-DSC scans upon the first heating and cooling ramps are shown below (Figure 1), and no difference is observed upon further cycling. It is observed that all scans present a hysteresis of several degrees between cooling and heating, which corresponds to the supercooling commonly observed upon nucleation of crystallized domains.[40] The major feature in these scans is the clear presence of two peaks upon cooling, at least up to $f = 0.62$. This is assigned to two different phase transitions, which have not been discriminated in previous reports on the $C_{13}COOH/C_{16}TA^+OH^-$ mixtures by Vautrin et al.[41] Upon heating, both transitions are less clearly resolved but are yet observable as a shoulder on a broader peak. Qualitatively, it is observed that both transitions are shifted to higher temperatures as f increases (enrichment in myristic acid), whereas the temperature shift between both transitions decreases and vanishes at $f = 0.67$, yielding one single transition. This strikingly occurs at the critical fraction mentioned above where the cohesive energy of the bilayer is so strong that no extraction by dialysis is possible.[28]

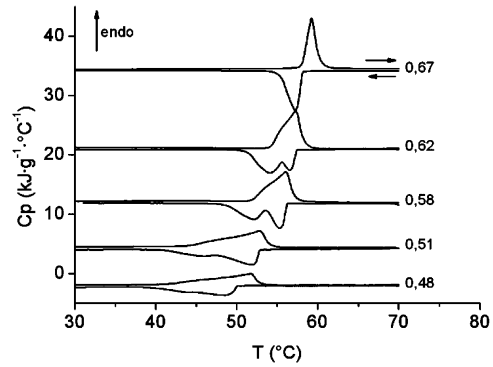

Figure 1. Typical DSC endotherms for myristic acid/C_{16}TAB mixtures at different myristic acid fractions. The scans have been displaced vertically for clarity.

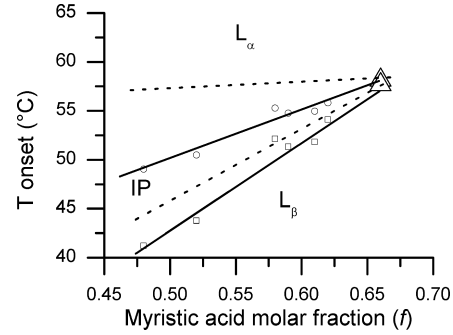

Figure 2. Onset temperature of each transition in the dialyzed $C_{13}COOH/C_{16}TAB$ mixtures as a function of the effective myristic acid molar fraction f. Triangles: single transition. The upper boundaries of each coexistence region (dotted lines) have been qualitatively inferred from the ^2H NMR spectra of the mixtures prepared with perdeuterated myristic acid (Figure 8). "IP" stands for "intermediate phase" (see text).

Even with no further quantitative analysis, it is already clear from the heating traces that no phase segregation with a preferential compound occurs at room temperature. Indeed, it would otherwise lead to a melting starting at a temperature independent of composition, characteristic for instance of a mixture showing an eutectic point. To extract more quantitative data, it is possible to deconvolute the peak into two contributions, apart from the $f = 0.67$ composition for which no second peak could be discriminated. This has been performed on the heating scans to avoid any effect related to supercooling. The ideal shape for a sharp transition is a straight slope followed by an exponential decay.[40] In practice, each individual transition can be fitted with a good approximation by a Gaussian curve centered at a given temperature T and standard deviation σ. The integral of the Gaussian provides the enthalpy of the transition, and the onset temperature T_{on} is approximated by $T - 2.15\sigma$, which sets the corresponding heat capacity at 10% of the maximum. It is therefore observed that the onset temperature of both transitions increase in the 40 °C−60 °C range as the effective molar fraction of myristic acid approaches $f = 0.66$ (Figure 2), until one single transition is observed. This trend is identical to the case of the $C_{13}COOH/C_{16}TA^+OH^-$ mixtures, although the lower temperature transition only was discriminated until now.[41] The exact nature of each transition is determined below.

The enthalpies per surfactant chain of each transition, as determined by the integral of the Gaussian, are given as a

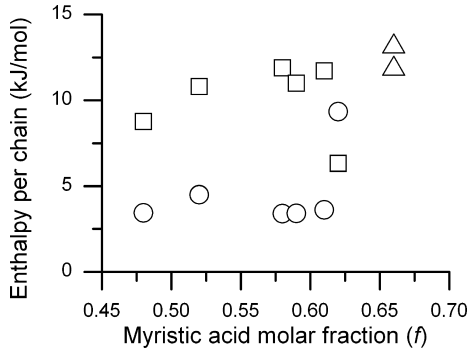

Figure 3. Enthalpy of each transition as a function of the molar fraction of myristic acid f as determined by a Gaussian deconvolution: (□) lower temperature transition, (○) higher temperature transition, and (△) single transition.

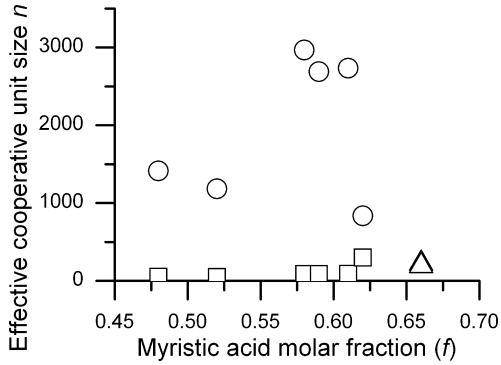

Figure 4. Effective cooperative unit size n as a function of myristic molar fraction f: (□) lower temperature transition, (○) higher temperature transition, and (△) single transition.

function of concentration above (Figure 3). The sum of both enthalpies is in the 15−18 kJ/mol range per surfactant chain, which is comparable to the enthalpy of fusion in phospholipids with comparable chain length.[42] The first transition is significantly more endothermic than the second transition. The ratio between both enthalpies is remarkably constant at all compositions, with $\Delta H_1/\Delta H_2 \sim 70/30$. This is a first indirect indication that both transitions correspond to two consecutive transitions of the same compound, instead of two different immiscible compounds undergoing one transition each. In the latter case, one would indeed expect the relative amount in each compound to vary with f, and therefore to observe a variation in $\Delta H_1/\Delta H_2$.

The width of each peak gives an indication on the "cooperativity" of a transition, that is, how close it is to a first-order transition.[35] The cooperativity can be estimated from the so-called effective cooperative unit size, which is the ratio of the enthalpy ΔH_{vH} derived from the Van't Hoff equation and the calorimetric enthalpy ΔH_{cal} determined by integration of the endotherms (see Methods):

$$n = \frac{\Delta H_{vH}}{\Delta H_{cal}}$$

For an ideal first-order transition, the endothermic peak would be infinitely sharp and the effective cooperative unit size is infinitely large. Experimentally, n takes finite values which give qualitative indications on the nature of both transitions (Figure 4). Apart from the cases where the two transitions are ill resolved or not resolved at all ($f = 0.62$ and 0.67), n is lower for the lower temperature transition by at least a factor of 20 ($n \approx 50-90$ against $n \approx 1100-3000$). The lower temperature transition is therefore significantly less cooperative than the higher temperature transition. Similar observations have been reported in phospholipids, for example, in phosphatidylcholines where the solid−solid pretransition between the L_β and P_β phases is less cooperative than the $P_\beta-L_\alpha$ main transitions.[42] More information about nature of the transitions in our system is provided by deuterium NMR performed on the analogue mixtures prepared with perdeuterated myristic acid.

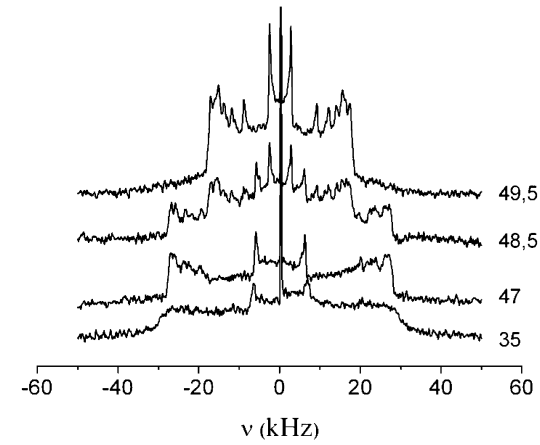

Figure 5. Deuterium NMR spectra of a dialyzed mixture of perdeuterated myristic acid and C_{16}TAB at $f = 0.59$ ($f_0 = 0.55$, dialyzed 3 days) at different temperatures, from bottom to top: 35, 47, 48.5, and 49.5 °C.

At low temperature (<35 °C), a broad spectrum ($\Delta\nu_{max} \approx 60$ kHz) is observed (Figure 5 and Supporting Information). The line assigned to isotopic water ($\nu = 0$ kHz) and the quadrupolar splitting assigned to the terminal $-CD_3$ groups of myristic acid ($\Delta\nu_{CD3} \approx 13$ kHz) are observed, but the resonances assignable to the CD_2 groups cannot be discriminated from each other. This spectrum is characteristic of vesicle bilayers in the gel phase (L_β, sometimes also referred to as V_β), where both the lateral diffusion of surfactants and the gauche−trans isomerization of the chains are strongly hindered.[36] This assignment is further confirmed by wide-angle X-ray scattering, as already reported previously for this system,[28,43,44] and small angle neutron scattering has also demonstrated that the in-plane relative distribution of both surfactants in the bilayer presents a short-range liquid order.[45] Above the higher-temperature phase transition (e.g., 49.5 °C in Figure 5), the spectrum width is significantly reduced ($\Delta\nu_{max} \approx 40$ kHz, $\Delta\nu_{CD_3} \approx 5$ kHz) and the individual quadrupolar splitting of each CD_2 group is resolved. This corresponds to an enhancement both in the lateral diffusion of the surfactant molecules and in the gauche−trans isomerization of the chains. This high-temperature spectrum is assigned to the complete melting of the vesicle bilayer (L_α or V_α phase).[36] The general shape of the spectra indicates that the fluid bilayers are aligned under the magnetic field, as usually observed.[46,47] At intermediate temperatures (e.g., 47 °C), the spectra share the features of both the L_β and L_α: the width of the various quadrupolar splitting remains as large as that in the L_β (e.g., $\Delta\nu_{max} \approx 55$ kHz and $\Delta\nu_{CD3} \approx 12$ kHz), but the peaks are well resolved, like in the L_α. This kind of spectrum is usually reported in mixtures of phospholipids with high contents of cholesterol and is classically assigned to the so-called "liquid ordered" phase (LO), that is, lipid chains with no gauche−trans isomerization but fast axially symmetric reorientations.[48,49] However, an alternative interpretation can also be considered,

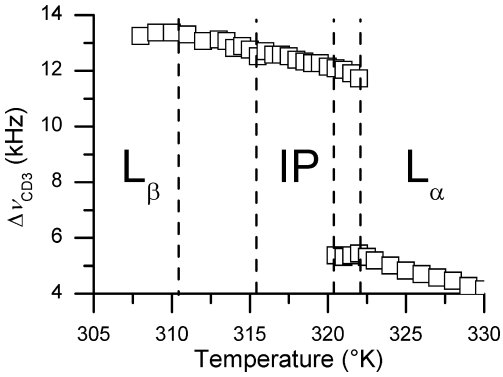

Figure 6. Quadrupolar splitting of the terminal CD_3 group as a function of temperature in a dialyzed perdeuterated $C_{13}COOH/C_{16}TAB$ sample at $f = 0.59$ ($f_0 = 0.55$, dialyzed 3 days).

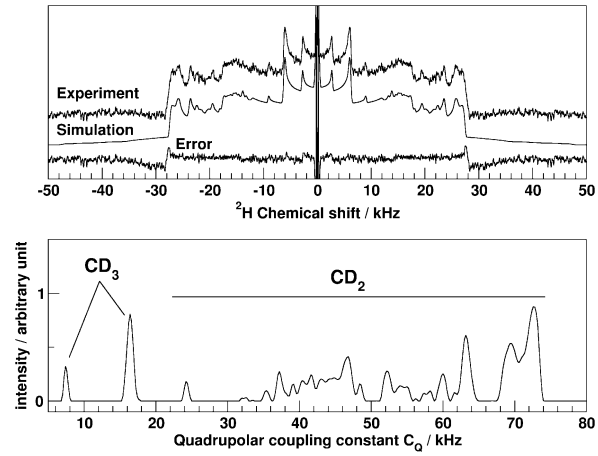

Figure 7. (top) Experimental and theoretical ^{2}H NMR spectra simulated with distribution of quadrupolar coupling constant (bottom) extracted using an inversion procedure (see text and eqs 1 and 2), for a mixture with $f = 0.62$ and 48.5 °C.

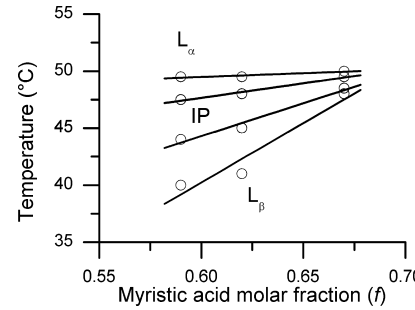

Figure 8. Phase diagram of the dialyzed perdeuterated $C_{13}COOH/C_{16}TAB$ mixtures as determined by ^{2}H NMR. The lines are linear fits through the experimental points.

that is, that gauche−trans isomerization occurs at given positions along the chain (corresponding to the positions where sharpening is observed on the spectra) but that no lateral diffusion is possible. This has already been proposed, for instance, in palmitic acid/palmitin mixtures presenting ^{2}H NMR spectra with identical features.[47] In practice, the nature of this "intermediate phase" (IP) does not affect the conclusion about lateral phase segregation, as discussed below. In any case, this intermediate phase has a detectable calorimetric signature. The first endothermic peak is assigned to the transition from the L_β to this intermediate phase and is less cooperative than the transition from this intermediate to the L_α phase (Figure 4).

Finally, at slightly higher temperatures, a superimposition of the spectra of the intermediate phase and the L_α is observed (e.g., 48.5 °C), which indicates a phase coexistence region after the second phase transition has started (above the solidus line), and before the melting is complete (below the liquidus line). The quadrupolar splittings assigned to the L_α phase decrease with temperature, which corresponds to an enhancement of mobility with temperature (Figure 6).

The two transitions observed by DSC are therefore assigned to a L_β−IP (intermediate phase) transition at low temperature and to a IP−L_α transition at higher temperature. Although shifted because of perdeuteration,[50] the onsets of the transitions at lower temperature and higher temperature as reported above for the perhydrogenated system (Figure 1) are therefore attributed straightforwardly to the upper phase boundaries of L_β and IP (corresponding to solidus lines), respectively. To establish a complete phase diagram, the upper limits of both coexistence regions (liquidus lines) are also required. In some cases, they can be determined from the offset temperature of the endotherms. However, this determination is usually not so straightforward because the transition kinetics is generally slower than the scan rate of the DSC, artificially leading to thermal events occurring even at temperatures above the liquidus line, where the single phase region is expected. This is obviously the case in this system as both endothermic peaks overlap, leading to offsets of the first peak at higher temperatures than the onset of the second peak.

As a consequence, alternative methods have been used to extract more information from the ^{2}H NMR spectra of the dialyzed perdeuterated $C_{13}COOH/C_{16}TAB$ system and extrapolate to the perhydrogenated case. The different phase boundaries can be directly determined from the signature of the different phases on the spectra. The lower boundaries of both coexistence regions and the upper boundary of the IP + L_α region are determined with a good confidence from the quadrupolar splitting of the terminal CD_3 groups (Figure 6). The upper boundary of the L_β + IP region is estimated, although with less confidence, from the linear combination of the spectra of both pure phases. The upper boundary of the IP + L_α region has also been completed using the lever rule and the relative fractions of IP and L_α phases as determined from integration of the oriented ("de-Paked") spectra at a given temperature and total composition f belonging to the IP + L_α region (Figure 7).

As a result, this provides the phase diagram of the dialyzed perdeuterated $C_{13}COOH/C_{16}TAB$ mixtures (Figure 8). It is observed that the positions of the upper phase boundaries of the L_β and IP are lowered by 8.5 °C with respect to the hydrogenated form (Figure 1) but the general shape remains unchanged. In particular, all boundaries tend to converge to a single point at $f \approx 0.67$ as the coexistence regions shrink out.

Discussion

The phase diagrams established above on both systems by different methods are only partial but share several features that allow drawing the same conclusion, which is the absence of segregation of a preferential compound of fixed composition at room temperature. Indeed, the phase diagrams present a L_β single-phase region at 25 °C in the explored range of compositions, instead of a coexistence region. The absence of phase separation at room temperature is supported by the absence of a thermal event below the "solidus" line, by the absence of a transition temperature independent of composition, by the absence of separate signature on the ^{2}H NMR spectra, and by the presence of a coexistence region which excludes the presence

of a directly adjacent two-phase region by the phase rule. Instead, $C_{13}COOH$ and CTA^+ are miscible at all compositions at least in the $f = 0.47-0.67$ range up to $T = 40$ °C and form bilayers in the gel state where the lateral in-plane distribution of both amphiphilic molecules shows a short-range order.[45]

The melting of the L_β phase occurs at higher temperatures as the mixture is enriched in myristic acid. A new phase transition was detected, which was unresolved in previous studies of the same system. The intermediate phase shows ^2H NMR spectra with broad quadrupolar splitting but showing also a series of sharper peaks at high quadrupolar splitting constants. Such spectra are usually interpreted as the signature of a liquid ordered (LO) phase that shows little gauche−trans isomerization but a higher lateral diffusion coefficient. However, alternative interpretations have already been proposed for such ^2H NMR spectra:[47] it has been suggested that gauche−trans isomerization can occur freely but that no lateral diffusion occurs. The exact nature of this intermediate phase is currently under investigation using direct structural determination.

Despite the absence of segregation of a preferential compound at room temperature, a $f = 0.67$ preferential ratio is observed which corresponds to the direct transition from the L_β to the L_α phase with no coexistence region. This behavior, that is, vanishing of the coexistence region at a preferential ratio but no demixing of a compound of this preferential ratio, is commonly observed in mixtures presenting an azeotrope composition.[51] More specifically, as the temperature of melting increases as the preferential ratio is approached, the $C_{13}COOH/CTA^+$ mixtures form a negative azeotrope, corresponding consistently to the case where the interaction between unlike molecules is more favorable than between identical molecules. Strikingly, this azeotrope composition coincides with the critical fraction of myristic acid above which dialysis becomes unable to extract surfactant by dialysis.[28] This indicates that this resistance to dialysis originates from an increase in the cohesion of the bilayer as the critical fraction is approached by extraction of the most soluble surfactant. This rules out the case where the bilayer initially consists of a mixture of a compound at a preferential composition and of the excess of surfactant which is then selectively extracted by the dialysis.

Another consequence of this absence of lateral phase separation concerns the morphology of the aggregates. It has been proposed previously that the segregation between a compound of preferential composition forming preferably planar bilayers and excess ionic surfactant forming preferably rims or pores controls the shape of the objects, that is, discs with equimolar bilayers and cationic rims for CTA-rich compositions ($f < 0.50$), and faceted vesicles with icosahedral shape presenting pores at the vertices for myristic acid-rich compositions ($f > 0.50$).[52] The results presented here demonstrate that the mechanism should be revised at least regarding the latter compositions and that no phase separation at the micrometer scale is observed, for example, like in some phospholipid vesicles.[53] The tentative demonstration of this segregation mechanism relied on the preferential adsorption of charged quantum dots on the vertices and edges of the faceted vesicles. It seems that this effect must be instead attributed to an increase in effective charge driven by curvature. Alternative mechanisms must then be proposed for the formation of such polyhedral vesicles, and possible answers can already be found in literature: although polyhedral vesicles have also been reported in the fluid state (octyltrimethylammonium perfluorooctanoate[54]), they are most often observed in vesicle crystallized surfactant bilayers.[30−33] This suggests that the formation of polyhedral vesicles with a discrete number of vertices could be driven, for instance, by the incompatibility between a spherical geometry and a bilayer with a tilt angle, as derived theoretically by Lubensky and Prost.[55] Structural defects must therefore be present but do not exist as a separate phase. Solving this question is both fundamentally appealing but also interesting as far as encapsulation and controlled delivery processes are concerned, as this topological incompatibility will create a given number of defects in the bilayer and therefore influence the permeability to solutes.

Conclusions

The composition/temperature phase diagrams of $C_{13}COOH/C_{16}TA$ mixtures and their perdeuterated analogues have been established with two complementary techniques in the fatty-acid-rich region. A phase unreported in the previous investigations has been detected at intermediate temperatures between the L_β and L_α phase, which shows unusual dynamic features. This phase diagram allows concluding that both surfactants are miscible at all compositions between $f = 0.47$ and 0.67 at room temperature and that no lateral segregation within the bilayer is therefore expected. Two major conclusions can be drawn from this observation: (i) the preferential composition that determines the resistance of the bilayers toward dialysis as reported before occurs from a continuous increase in the cohesion of the bilayer upon surfactant extraction (instead of a selective extraction of the surfactant in excess with respect to a preferential compound), and (ii) the morphology of the polyhedral vesicles is not determined by lateral phase segregation in the bilayer, but an alternative mechanism must be proposed.

Supporting Information Available: The effective molar fraction of myristic acid (f) as a function of the initial fraction f_0 and the time of dialysis, and ^2H NMR spectra as a function of temperature at $f = 0.59$. This material is available free of charge via the Internet at http://pubs.acs.org.

References and Notes

(1) Kaler, E. W.; Herrington, K. L.; Murthy, A. K.; Zasadzinski, J. A. N. *J. Phys. Chem.* **1992**, *96*, 6698–6707.
(2) Zemb, T.; Carriere, D.; Glinel, K.; Hartman, M.; Meister, A.; Vautrin, C.; Delorme, N.; Fery, A.; Dubois, M. *Colloids Surf., A* **2007**, *303*, 37–45.
(3) Hao, J. C.; Hoffmann, H. *Curr. Opin. Colloid Interface Sci.* **2004**, *9*, 279–293.
(4) Khan, A.; Marques, E. F. *Curr. Opin. Colloid Interface Sci.* **1999**, *4*, 402–410.
(5) Kronberg, B. *Curr. Opin. Colloid Interface Sci.* **1997**, *2*, 456–463.
(6) Jokela, P.; Jonsson, B.; Khan, A. *J. Phys. Chem.* **1987**, *91*, 3291–3298.
(7) Tondre, C.; Caillet, C. *Adv. Colloid Interface Sci.* **2001**, *93*, 115–134.
(8) Zemb, T.; Dubois, M. *Aust. J. Chem.* **2003**, *56*, 971–979.
(9) Zhu, B. Y.; Rosen, M. J. *J. Colloid Interface Sci.* **1984**, *99*, 435–442.
(10) Lucassen-Reynders, E. H.; Lucassen, J.; Giles, D. *J. Colloid Interface Sci.* **1981**, *81*, 150–157.
(11) Li, X. F.; Kunieda, H. *Curr. Opin. Colloid Interface Sci.* **2003**, *8*, 327–336.
(12) Sierra, M. B.; Morini, M. A.; Schulz, P. C.; Ferreira, M. L. *Colloid Polym. Sci.* **2005**, *283*, 1016–1024.
(13) Jost, F.; Leiter, H.; Schwuger, M. J. *Colloid Polym. Sci.* **1988**, *266*, 554–561.
(14) Li, H. G.; Hao, J. C. *J. Phys. Chem. B* **2008**, *112*, 10497–10508.
(15) Song, A. X.; Dong, S. L.; Jia, X. F.; Hao, J. C.; Liu, W. M.; Liu, T. B. *Angew. Chem., Int. Ed.* **2005**, *44*, 4018–4021.
(16) Holland, P. M.; Rubingh, D. N. *J. Phys. Chem.* **1983**, *87*, 1984–1990.
(17) Bergstrom, M.; Eriksson, J. C. *Langmuir* **2000**, *16*, 7173–7181.
(18) Hines, J. D. *Curr. Opin. Colloid Interface Sci.* **2001**, *6*, 350–356.
(19) Herrington, K. L.; Kaler, E. W.; Miller, D. D.; Zasadzinski, J. A.; Chiruvolu, S. *J. Phys. Chem.* **1993**, *97*, 13792–13802.
(20) Shiloach, A.; Blankschtein, D. *Langmuir* **1998**, *14*, 1618–1636.

(21) Villeneuve, M.; Kaneshina, S.; Imae, T.; Aratono, M. *Langmuir* **1999**, *15*, 2029–2036.
(22) Kato, T.; Takeuchi, H.; Seimiya, T. *J. Phys. Chem.* **1992**, *96*, 6839–6843.
(23) Caillet, C.; Hebrant, M.; Tondre, C. *Langmuir* **2000**, *16*, 9099–9102.
(24) Bergstrom, M.; Pedersen, J. S. *J. Phys. Chem. B* **2000**, *104*, 4155–4163.
(25) Brasher, L. L.; Kaler, E. W. *Langmuir* **1996**, *12*, 6270–6276.
(26) Bergstrom, M. *Langmuir* **2001**, *17*, 993–998.
(27) Yuet, P. K.; Blankschtein, D. *Langmuir* **1996**, *12*, 3802–3818.
(28) Michina, Y.; Carriere, D.; Mariet, C.; Moskura, M.; Berthault, P.; Belloni, L.; Zemb, T. *Langmuir* **2009**, *25*, 698–706.
(29) Kopetzki, D.; Michina, Y.; Gustavsson, T.; Carriere, D. *Soft Matter* **2009**, *5*, 4212–4218.
(30) Dubois, M.; Deme, B.; Gulik-Krzywicki, T.; Dedieu, J. C.; Vautrin, C.; Desert, S.; Perez, E.; Zemb, T. *Nature* **2001**, *411*, 672–675.
(31) Regev, O.; Marques, E. F.; Khan, A. *Langmuir* **1999**, *15*, 642–645.
(32) Antunes, F. E.; Brito, R. O.; Marques, E. F.; Lindman, B.; Miguel, M. *J. Phys. Chem. B* **2007**, *111*, 116–123.
(33) Antunes, F. E.; Marques, E. F.; Gomes, R.; Thuresson, K.; Lindman, B.; Miguel, M. G. *Langmuir* **2004**, *20*, 4647–4656.
(34) Vautrin, C.; Zemb, T.; Schneider, M.; Tanaka, M. *J. Phys. Chem. B* **2004**, *108*, 7986–7991.
(35) Heinz, H.; Sturtevant, J. *J. Biol. Chem.* **1972**, *247*, 6071–6075.
(36) Davis, J. H. *Biochim. Biophys. Acta* **1983**, *737*, 117–171.
(37) Schafer, H.; Madler, B.; Sternin, E. *Biophys. J.* **1998**, *74*, 1007–1014.
(38) Tikhonov, A.; Arsenin, V. *Solutions of Ill-Posed Problems*; John Wiley: New York, 1997.
(39) Angeli, F.; Delaye, J.-M.; Charpentier, T.; Petit, J.-C.; Ghaleb, D.; Faucon, P. *J. Non-Cryst. Solids* **2000**, *276*, 132–144.
(40) Gray, A. P. In *Analytical Calorimetry*; Porter, R. F., Johnson, J. M., Eds.; Plenum Press: New York, 1968; Chapter: A Simple Generalized Theory For The Analysis Of Dynamic Thermal Measurement, pp 209−218.
(41) Vautrin, C.; Dubois, M.; Zemb, T.; Schmolzer, S.; Hoffmann, H.; Gradzielski, M. *Colloids Surf., A* **2003**, *217*, 165–170.
(42) Koynova, R.; Caffrey, M. *Biochim. Biophys. Acta, Biomembr.* **1998**, *1376*, 91–145.
(43) Maurer, E.; Belloni, L.; Zemb, T.; Carriere, D. *Langmuir* **2007**, *23*, 6554–6560.
(44) Zemb, T.; Dubois, M.; Deme, B.; Gulik-Krzywicki, T. *Science* **1999**, *283*, 816–819.
(45) Carriere, D.; Belloni, L.; Demé, B.; Dubois, M.; Vautrin, C.; Meister, A.; Zemb, T. *Soft Matter* **2009**, *5*, 4983–4990.
(46) Alam, T. M.; McIntyre, S. K. *Langmuir* **2008**, *24*, 13890–13896.
(47) Douliez, J. P. *Langmuir* **2004**, *20*, 1543–1550.
(48) Vist, M. R.; Davis, J. H. *Biochemistry* **1990**, *29*, 451–464.
(49) Ipsen, J. H.; Karlstrom, G.; Mouritsen, O. G.; Wennerstrom, H.; Zuckermann, M. J. *Biochim. Biophys. Acta* **1987**, *905*, 162–172.
(50) Aussenac, F.; Laguerre, M.; Schmitter, J. M.; Dufourc, E. *Langmuir* **2003**, *19*, 10468–10479.
(51) Moore, W. *Physical Chemistry*; Prentice Hall: Englewood Cliffs, New Jersey, 1962.
(52) Dubois, M.; Lizunov, V.; Meister, A.; Gulik-Krzywicki, T.; Verbavatz, J. M.; Perez, E.; Zimmerberg, J.; Zemb, T. *Proc. Natl Acad. Sci. U.S.A.* **2004**, *101*, 15082–15087.
(53) Baumgart, T.; Hess, S. T.; Webb, W. W. *Nature* **2003**, *425*, 821–824.
(54) Gonzalez-Perez, A.; Schmutz, M.; Waton, G.; Romero, M. J.; Krafft, M. P. *J. Am. Chem. Soc.* **2007**, *129*, 756–757.
(55) Lubensky, T. C.; Prost, J. *J. Phys. II* **1992**, *2*, 371–382.

JP910267V